

Josephson coupling in high- T_c superconducting junctions using ultra-thin BaTiO₃ barriers

H. Navarro,^{1,†} M. Sirena,^{1,2} Jeehoon Kim,^{3,4,5} N. Haberkorn.^{1,2}

¹ Instituto Balseiro, Universidad Nacional de Cuyo and Comisión Nacional de Energía Atómica, Av. Bustillo 9500, 8400 San Carlos de Bariloche, Argentina.

² Comisión Nacional de Energía Atómica and Consejo Nacional de Investigaciones Científicas y Técnicas, Centro Atómico Bariloche, Av. Bustillo 9500, 8400 San Carlos de Bariloche, Argentina.

³ Department of Physics, Pohang University of Science and Technology, Pohang 37673, Republic of Korea.

⁴ Advanced Material Science, Pohang University of Science and Technology, Pohang 37673, Republic of Korea.

⁵ Max Planck POSTECH Center for Complex Phase Materials, Pohang University of Science and Technology, Pohang 37673, Republic of Korea.

Corresponding Author

*E-mail: hnavarro@physics.ucsd.edu

Present Address

†Department of Physics and Center for Advanced Nanoscience, University of California, San Diego, La Jolla, California 92093, USA.

ABSTRACT.

We study the electrical transport of vertically-stacked Josephson tunnel junctions using GdBa₂Cu₃O_{7- δ} electrodes and a BaTiO₃ barrier with thicknesses between 1 nm and 3 nm. The junctions with an area of 20 μ m x 20 μ m were fabricated combining optical lithography and ion etching using GdBa₂Cu₃O_{7- δ} (16 nm) / BaTiO₃ (1 - 3 nm) / GdBa₂Cu₃O_{7- δ} (16 nm) trilayers growth by sputtering on (100) SrTiO₃. Current-voltage measurements at low temperatures show a Josephson coupling for junctions with BaTiO₃ barriers of 1 nm and 2 nm. Reducing the barrier thickness below a critical thickness seems to suppress the ferroelectric nature of the BaTiO₃. The Josephson coupling temperature is strongly reduced for increasing barrier thicknesses, which may be related to the suppression of the superconducting critical temperature in the bottom GdBa₂Cu₃O_{7- δ} due to stress. The Josephson energies at 12 K are of \approx 1.5 mV and \approx 7.5 mV for BaTiO₃ barriers of 1 nm and 2 nm. Fraunhofer patterns are consistent with fluctuations in the critical current due to structural inhomogeneities in the barriers. Our results are promising for the development of Josephson junctions using high- T_c electrodes with energy gaps much higher than those usually present in conventional low-temperature superconductors.

Keywords: Josephson junctions, high- T_c superconductors, thin films.

1. Introduction

There has been continuous progress in superconductor electronics fabrication towards incorporating materials allowing faster operation speeds, reducing the influence of thermal noise and reducing the minimum size of circuit features [1,2]. Josephson junctions (JJs) based on high-transition-temperature superconductors (HTS) are of technological relevance for many applications going from high-performance computing to high-frequency sensors. The main advantage of HTS over conventional low-temperature superconductors (LTS) is related to the large superconducting gap and high critical temperature (T_c), which traduces in devices with high-frequency operation rates and low thermal noise (I_N) [3]. Most research in HTS JJs is related to planar arrays of junctions produced by mechanical break [4] and grain boundaries [5,6,7]. Reports on vertically-stacked JJ using HTS are scarcer in the literature [8,9,10,11]. By contrasting planar with vertically-stacked JJs, the latter allow to include barriers with different electrical and magnetic properties [12,13], and to tune critical currents changing the barrier thickness in atomic scales [14]. However, these advantages are conditioned by the 3D growth mechanism usually observed in HTS thin films [15] and by the limitations to fabricate barriers with well-defined nanoscale interfaces [16,17].

Recently, we reported Josephson coupling in superconductor–insulator–superconductor (SIS) fabricated with $\text{GdBa}_2\text{Cu}_3\text{O}_7$ (GBCO) electrodes and a SrTiO_3 barrier [11]. The junctions display high characteristic voltages $V_C = I_c R_n$ (with I_c the critical current and R_n , the resistance at the normal state) above those typically observed in those fabricated with LTS [18] and MgB_2 [19]. We have found that changing the barrier thickness affects not only the Josephson junction energy, through changes in both the I_c and R_n , but also the Josephson temperature. Because materials with a perovskite structure usually display a broad range of physical properties, it may be interesting to extend the study to other barriers. Indeed, new functionalities may be obtained using ferromagnetic [20,21] or ferroelectric materials [13,22,23,24]. In ferromagnetic JJs, so-called pi junctions, the phase of the junction can be set to either 0 or pi depending on the thickness of the ferromagnetic layer [25]. On the other hand, two different effects could be expected for a ferroelectric JJs, which is related to the tuning of the critical current. The first is associated with the influence of the polarization on the superconducting properties of the electrodes [23,26]. The second is related to the tuning of the barrier thickness by polarization [27].

In this work, we investigated Josephson coupling in tunnel junctions fabricated using $\text{GdBa}_2\text{Cu}_3\text{O}_{7-\delta}$ (GBCO) as electrodes and BaTiO_3 (BTO) as an insulator barrier. The motivation of this work was studying the influence of a potential ferroelectric barrier on the characteristic current-voltage (IV) curves of JJs at low temperatures. GBCO is a superconducting material with critical temperature $T_c \approx 93$ K. BTO is a ferroelectric material with a Curie temperature of ≈ 390 K in bulk. For thin films, the transition temperature suppresses as thickness decreases and vanishes at approximately 2 nm [28,29]. GBCO has an orthorhombic structure with lattice parameters of $a = 0.383$ nm, $b = 0.389$ and $c = 1.17$ nm. BTO is a cubic perovskite with $a = 0.399$ nm. Based in our previous work of GBCO/ SrTiO_3 /GBCO junctions [11],

the GBCO thickness of the 16 nm was fixed by considering a trade-off between T_c and the presence of smooth surfaces [15]. The BTO thickness was varied between 1 nm and 3 nm. We analyze the junctions by performing IV curves at low temperatures. The presence of Josephson coupling was confirmed from the response of the critical current I_c as a function of the magnetic field (Fraunhofer patterns). The results are discussed considering inhomogeneous barriers produced by thickness fluctuations and interface disorder.

2. Experimental

GBCO/BTO/GBCO trilayers were grown on (100) SrTiO₃ by sputtering as described in detail elsewhere [15,30,31]. The tunnel junctions were designed using 16 nm thick GBCO electrodes and a BTO barrier with a thickness (d_{BTO}) of 1 nm, 2 nm, 3 nm, and 4 nm. During the deposition, the substrate was fixed to the sample holder using silver paint and kept at 730°C in an Ar (90%) / O₂ (10%) mixture at a pressure of 400 mTorr. The GBCO and BTO layers were grown using 25 W by DC and RF sources, respectively. After deposition, the temperature decreases in two steps. First, the sample holder is cold down to 500°C, and the O₂ pressure increases to 100 Torr. Second, the sample is cold- down to room temperature at a rate of 1.5° C/min. A 2 nm thick STO buffer layer was introduced to reduce the formation of 3D defects in the bottom electrode [15]. Wherever used, the notations [G- d_{BTO} -G] indicate a GBCO bottom and top electrodes and a BTO barrier with a thickness d (nm).

X-ray diffraction (XRD) data were obtained using a Panalytical Empyrean diffractometer operated at 40 kV and 30 mA with the Cu_{K α} radiation. The structural analysis was performed based on Θ -2 Θ scans with an angular resolution of 0.02°. The thicknesses of the GBCO and BTO layers were estimated from low angle X-ray reflectivity (XRR) measurements (not shown). Atomic force microscopy (AFM) images were obtained in tapping mode with a Dimension 3100 ©Brucker microscope. RMS values correspond to the root mean square average of height deviation taken from the mean image data plane.

Tunnel junctions with an area of 400 μm^2 were fabricated according to the steps previously described in reference [11]. Figure 1a shows a schematic diagram of a [G- d_{BTO} -G] junction. Before starting with the micro-fabrication process, the sample is covered with 60 nm of silver by sputtering (to avoid surface damage in the top electrode). The fabrication process is as follows: 1-2) using photoresist positive and ion milling we create a bridge with a length of 2 mm and a width of $\approx 70 \mu\text{m}$ (removing all the sample) and square pillars (20 μm x 20 μm) on the top of the bridge (removing only the top electrode), respectively; 3) positive photoresist is used to create a square pillar of 10 μm x 10 μm on the center of the pillars generated at the first step; 3) the junction is covered with ≈ 100 nm thick SiO₂ film by RF sputtering; 4) the area of 10 μm x 10 μm on the top of the junction is open by lift-off process removing the remaining photoresist using acetone; and, 5) a path of silver is deposited by sputtering on the SiO₂ capping layer (including the open area of 10 μm x 10 μm) to facilitate electrical connections. Figure 1b shows a picture

with the configuration used to make electrical contacts in which the path of silver crosses the junction. Figures 1cd show an AFM image and a height profile of the square pillar developed in the steps 1 and 2 mentioned above.

The process to obtain the characteristic current-voltage (IV) curves is similar to the described in reference [11]. The measurements were obtained using the standard four-point geometry. Each point in the curves is the average of 50 measures. A copper coil is used to perform IV curves as a function of the magnetic field. We define the Josephson coupling temperature (T_J) as the temperature where the Josephson Effect disappears.

3. Results and discussion

Figure 2 shows the XRD patterns for a pure GBCO film, and [G- d_{BTO} -G] trilayers with $d = 1$ nm, 2 nm, and 3 nm. The XRD patterns of the single GBCO layer display the (00l) reflections, indicating epitaxial growth with c -axis orientation. The rocking curve for the (005) GBCO line exhibit a full width at half maximum values of $0.35(5)^\circ$ [15]. The trilayers with $d = 2$ nm and 3 nm show the reflection (002) of the BTO layer at $2\theta \approx 43.1^\circ$ and 43.7° . The out-plane lattice parameters are $a = 0.420$ nm ($d = 2$ nm) and 0.414 nm ($d = 3$ nm), indicating that the BTO layer is strained (compressed in the plane). The (002) reflection of the BTO is not distinguishable from the background for $d = 1$ nm, which can be related to the influence of the size in the peak width.

Figure 3 shows the evolution of the surface topology by adding the successive layers measured by AFM in [G-2-G]. The bottom GBCO electrode displays smooth surfaces with a roughness average (Ra) of around 0.7 nm (expressed as root mean square (RMS)) [11]. Typically, GBCO thin films display RMS ≈ 0.5 nm. The roughness in the films increases adding the BTO and GBCO capping layers. The GBCO / BTO bilayers show a surface topology with uniform terraces and some 3D defects mainly originated in defects coming from the bottom electrode [31,32]. The borders of 3D defect usually display higher electrical conductivity than terraces increasing the inhomogeneity in the properties of barrier [30,31]. The electrical conductivity across the barrier decreases as the thickness increases. IV curves performed at room temperature show that tunneling and oxygen vacancy migration (OVM) contribute to the conductivity in BTO barriers [32]. The latter suppresses as the temperature reduces [33]. It should be noted that, although the roughness in the GBCO capping layer is irrelevant for the practical ends of the joint, we have found that the inhomogeneous thickness makes more complicated its removal by ion milling during the fabrication of the junction (step 2 described above).

Figure 4 shows the IV curves of JJ with ultra-thin BTO barriers. The JJs with $d = 1$ nm and 2 nm show Josephson coupling with T_J of approximately 77 K and 41 K, respectively. The suppression of T_J may be associated with both a thicker insulator layer reducing the superconducting wave-function overlap and a

lower T_c in the bottom GBCO electrode [11,31]. The R_N values (see criterion in Fig. 4a) are of 0.5Ω ($d = 1$ nm) and 115Ω ($d = 2$ nm). The IV curves for [G-3-G] show features related to superconductivity for temperatures lower than 40 K. However, as we previously discussed for a 3 nm thick STO barrier [11], no low field interference effect in the critical current was observed for this sample, ruling out the presence of a Josephson coupling between the superconducting electrodes. In addition, the IV curves in [G-3-G] display a hysteretic behavior at high polarizations (see dotted circle). This effect may be related to OVM [33]. The barrier thickness ($d \leq 2$ nm) in which the Josephson coupling appears using BTO is similar to the previously reported for STO [11], consistent with the short coherence length ξ of the GBCO [34]. The IV curves for [G-1-G] and [G-2-G] display hysteresis, which is a distinctive feature of SIS junctions and is usually called underdamped behavior [35]. There are not ferroelectric features such as hysteretic behavior at the normal state or a step due to resistive switching [23,27,33]. It is important to mention that, although the presence of FE may be affected by the structural disorder, the Josephson coupling disappears for barriers thicker than 2 nm being closer to the limit in which the ferroelectricity vanishes [36].

For further characterization of the junctions, we analyze the critical current I_c as a function of the magnetic field (H). For a rectangular junction with uniform current density,

$$I_c(H) = I_0 \left| \frac{\sin\left(\frac{\pi H}{H_0}\right)}{\frac{\pi H}{H_0}} \right|, \quad [\text{eq. 1}]$$

here $I_0 = J_f WL$ (J_f the total current density, W and L the lengths of the junction), H_0 is the value of the magnetic field corresponding to a flux quantum penetrating into the junction [35]. Figure 5 shows $I_c(H)$ for [G-1-G] for $T = 12$ K, 25 K and 50 K. Each point corresponds to an IV curve performed at a fixed H . The criteria for I_c and R_n determination are indicated in Fig. 4a. The curves display the expected modulation for Josephson coupling with minima spacing each $\Delta H \approx 30$ Oe (see dotted lines in Fig. 5). Similar patterns were obtained for STO barriers [11]. Using equation 1, ΔH takes place at $\phi_0 = \Delta H \cdot A_{\text{effective}} = 30 \cdot L \cdot d$ with $L = 20 \mu\text{m}$ for our junctions and $\phi_0 = 2.07 \cdot 10^{-7} \text{ G} \cdot \text{cm}^{-2}$, and corresponds to $d \approx 35$ nm. The latter agrees with the total thickness of the junctions (electrodes with thicknesses of ≈ 16 nm and a BTO barrier of $\approx 1-2$ nm), which is much smaller than the penetration depth λ in GBCO ($\lambda \approx 120$ nm [34]).

Although the magnetic field response of the junctions displays a qualitative agreement with the predicted by equation 1, a distinctive feature is a residual current at the minima. The origin of this anomaly in the patterns may be related to thickness fluctuations in the BTO layer and inhomogeneous current distribution in the junctions (see Figs 3ab) [11,37,38]. This assumption agrees with conductivity maps obtained at room temperature in GBCO / BTO bilayers indicates that there are fluctuations mainly originated by the presence of topological defects in the bottom GBCO electrode [31]. For inhomogeneous barriers with residual currents at the minima where the thickness fluctuations are small in comparison with the thickness of the barrier, the Fraunhofer pattern has been described by

$$I_c(H) = \sqrt{\left(I_0^2 - \frac{\bar{I}_1^2}{\pi N}\right) \left(\frac{\sin \frac{\pi H}{H_0}}{\frac{\pi H}{H_0}}\right)^2 + \frac{\bar{I}_1^2}{\pi N}}, \quad [\text{eq. 2}]$$

where \bar{I}_1^2 is the mean-square of the current fluctuations across the barrier and N is a factor that represent the thickness fluctuation ($N > 1$ for small fluctuations) [37]. The fits need to considers a factor $\gamma^2 = \left(\frac{\bar{I}_1^2}{I_0^2}\right) \left(\frac{1}{\pi N}\right)$. The data for [G-1-G] at 12 K, 25 K and 50 K reproduce with $\gamma \approx 0.13$, indicating that the mechanism is the same for the three temperatures (see straight lines in Fig. 5).

Figure 6 shows the temperature dependence of V_c for [G-1-G] and [G-2-G]. For comparison, data of reference [11] for HTS and STO barriers with similar thicknesses are included. For SIS with identical superconductors, the theoretical temperature dependence of V_c is limited by the superconducting gap as

$$V_c = I_c R_n = \frac{\pi \Delta(T)}{2e} \tanh \frac{\Delta(T)}{2kT}, \quad [\text{eq. 3}]$$

where $\Delta(T) = \Delta(0) \tanh \left\{ 1.82 \left[1.018 \left(\frac{T_c}{T} - 1 \right) \right]^{0.51} \right\}$ [39] and $\Delta(0) = 1.76kT_c$. Our analysis does not consider non-monotonic effects in the $I_c(T)$ curves usually associated with d -wave superconductors [40]. The Josephson energies at 12 K are of ≈ 1.5 mV and ≈ 7.5 mV for BTO barriers with a thickness of 1 nm and 2 nm. These values are strongly affected by the large change in the R_N values of the JJs. As we mentioned above, the R_N value decrease's from 115 Ω for $d = 2$ nm to 0.5 Ω for $d = 1$. The low R_N for $d = 1$ infers that the electrode is not fully covered, suggesting the coexistence of SIS and superconductor–normal –superconductor regions (SNS). The $V_c(T)$ dependences decrease systematically to reach zero at T_J of ≈ 77 K and ≈ 41 K for $d = 1$ and $d = 2$, respectively. Tunnel junctions with BTO and STO display the same features in V_c and T_J . The devices with 1 nm thick barriers exhibit more substantial discrepancies than the samples with thicker barriers. This effect may be related to the higher influence of fluctuations in the barrier thickness and interface effects on the properties of ultra-thin barriers (coexistence of conducting and insulator regions). Moreover, as in STO layers, even for a low T_J , the best performance is found for the thicker barrier where low density of pinholes and conducting regions are expected [11,31].

The large Josephson energy for the samples reported here and in reference [11] is evidenced in the low thermal noise of the IV curves. The value of $V_c(12 \text{ K}) \approx 7.5$ mV is larger than that generally observed in NbN [18] and MgB2 [19,41] tunnel junctions. Among nitrides, NbN displays the maximum $\Delta(0)$ with a theoretical limit of $V_c \approx 4$ mV. On the other hand, a value of ≈ 2 mV has been experimentally reported for MgB₂ [19,41]. Moreover, the Josephson energies using BTO and STO barriers result in higher than those reported in planar junctions [42,43]. Even considering that T_J in our junctions reduces as barrier thickness

increases, the high V_c values offer several advantages for operation at low temperatures. Indeed, the quantum effects tend to wash out as a consequence of thermal noise when the operation temperature is increased, indicating that low operating temperatures are desired even for JJ with HTS. As we mentioned above, a high Josephson energy is essential for the development of high-quality JJ for two factors, reduced influence of thermal noise and a higher operating frequency.

Our results in Josephson junctions fabricated using HTS and insulator barriers such as BTO and STO have demonstrated similar behavior [11]. We found that at low temperatures, the JJs display higher V_c as the barrier thickness increases. The Josephson coupling usually vanishes as the barrier thickness increases to 2 nm, which is consistent with the short coherence length ξ of the HTS. The high V_c values displayed by vertically-stacked JJ using HTS is promising for applications in electronic systems that require a high-frequency operation. As a side note, two points should be considered towards improving the performance of our results. First, higher I_c values should be obtained for 2 nm thick insulator barriers increasing T_c in the bottom electrode, this should increase the Josephson energy of the Junctions further improving its operating frequency and reducing the influence of thermal noise. Second, it is essential to note that the properties in ultra-thin films based on perovskites usually are affected by interface disorder. This fact implies a technological challenge associated with the optimization of the interfaces to conserve bulk properties or to generate new ones in the nanometer scale.

4. Conclusions

We characterized the Josephson coupling in HTS junctions using ultra-thin BaTiO₃, which is an essential step towards the integration of perovskite barriers in superconducting JJ. The results show that tunnel junctions with a barrier thickness of 1 nm and 2 nm display the expected behavior for the Josephson Effect. The critical barrier thickness for ferroelectric effects in these systems is usually higher than 2 nm. The Josephson energies at 12 K are of $\gg 1.5$ mV and $\gg 7.5$ mV for BaTiO₃ barriers of 1 nm and 2 nm. Fraunhofer patterns are consistent with fluctuations in the critical current due to inhomogeneities in the insulator barrier. The present experiments show Josephson coupling with energies above the theoretical limits for LTS and similar to the expectations for ideal junctions with MgB₂. When searching for new functionalities using perovskite compounds with different physical properties (i.e. ferroelectric or ferromagnetic barriers), special care should be taken oriented to optimize their properties at the nanoscale.

Acknowledgements

This work was partially supported by the ANPCYT PICT 2015-2171 and 2018-03126. Jeehoon Kim was supported by the National Research Foundation of Korea (NRF) and the Korea government (MSIT) (grants 2016K1A4A4A01922136, 2018R1A5A6075964, 2019R1A2C2090356). MS and NH are members of the Instituto de Nanociencia y Nanotecnología CNEA-CONICET (Argentina).

Figure 1. *a)* Schematic diagram of a $[G-d_{\text{BTO}}-G]$ junction. *b)* Image of the tunnel junction and the silver path used to facilitate the electrical contacts in the top GBCO electrode. *c)* AFM image and a height profile of the square pillar after remove the top GBCO electrode.

Figure 2. X-ray diffraction patterns (logarithmic intensity scale) of a 16 nm thick GBCO films and $[G-d_{\text{BTO}}-G]$ trilayers with $d = 1$ nm, 2 nm, and 3 nm. The measurements were performed at room temperature.

Figure 3. $10 \times 10 \mu\text{m}^2$ topographical images with the surface evolution including a 16 nm thick GBCO thin with the successive addition of a 2 nm thick BTO insulator barrier and a 16 nm GBCO capping layer. Surface roughness height profiles are included.

Figure 4. Characteristic IV curves at different temperatures for *a)* $[G-1-G]$; *b)* $[G-2-G]$; and, *c)* $[G-3-G]$. Measurements are performed applying current and measuring voltage. Josephson coupling is observed for JJ with BTO barriers of 1 nm and 2 nm. The criteria for the determination of I_c and R_n are indicated in *a)*. The inset panel *a)* corresponds to a zoom of the IV curve at 76 K. The arrows in the hysteretic regions of the curves indicate the direction in the measurements.

Figure 5. I_c modulation by an external magnetic field for $[G-1-G]$ at *a)* 12 K; *b)* 25 K; and, *c)* 50 K. The dotted and straight lines correspond to the fit for an ideal Josephson junction using equation 1 and equation 2, respectively.

Figure 6. Comparison of V_c measured in $[G-1-G]$ and $[G-2-G]$ with the theoretical expectations according to the equation 2. The dashed lines correspond to the expected values considering T_J of 42 K and 76 K. Data for JJ with STO barriers of 1 nm and 2 nm from reference [11] are included.

Figure 1.

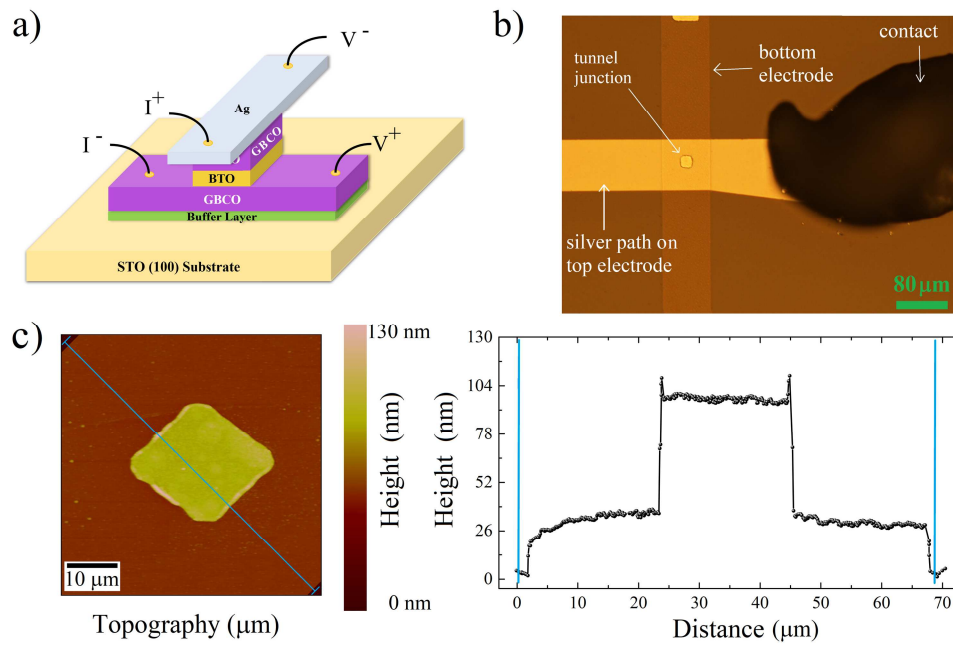


Figure 2.

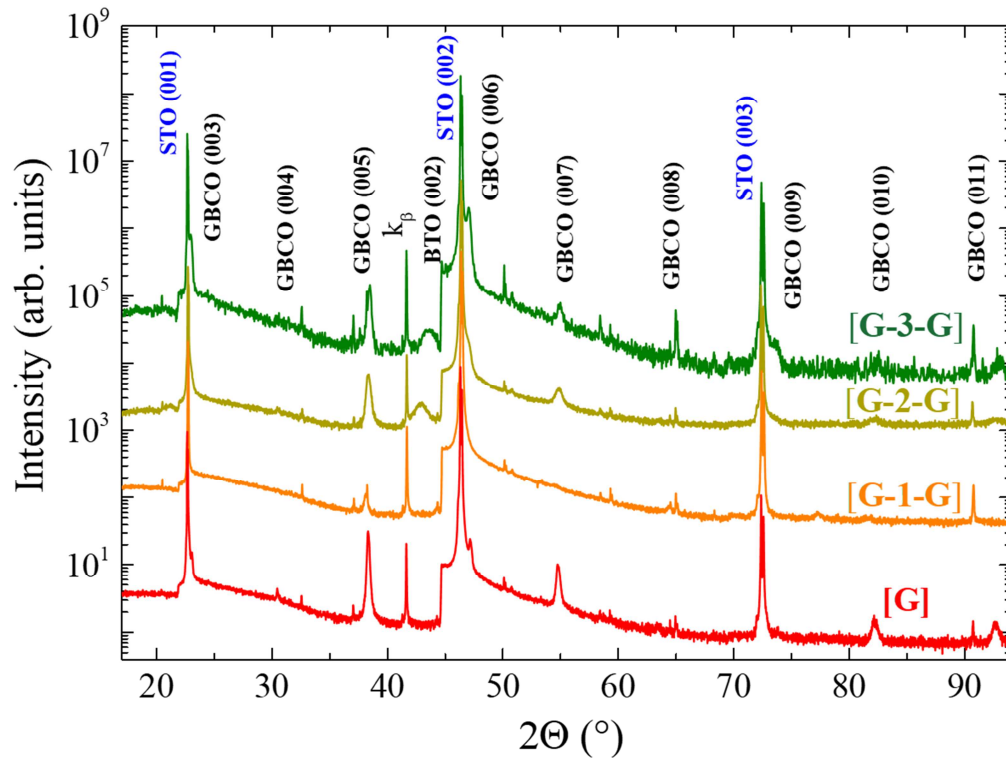


Figure 3.

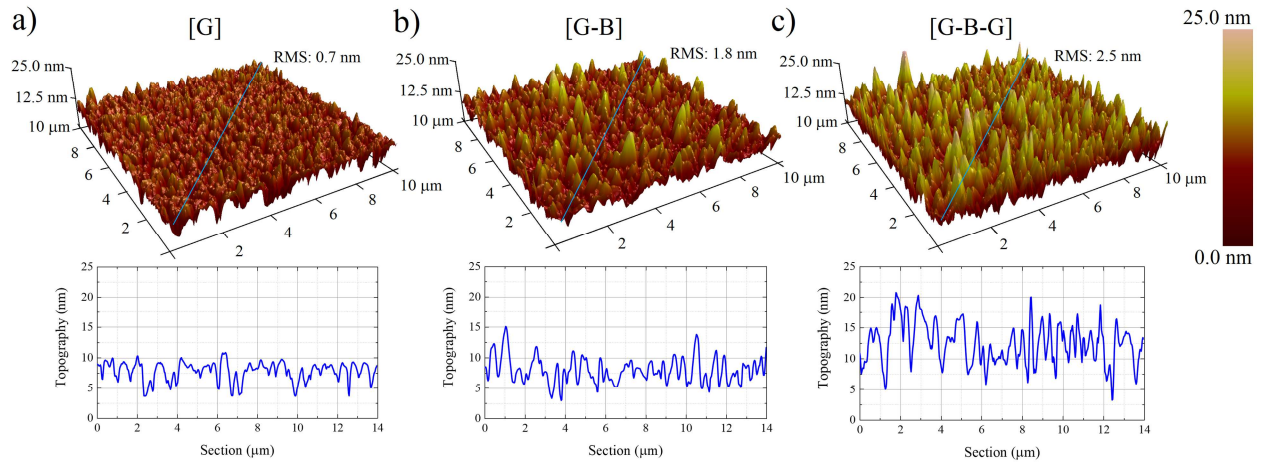


Figure 4.

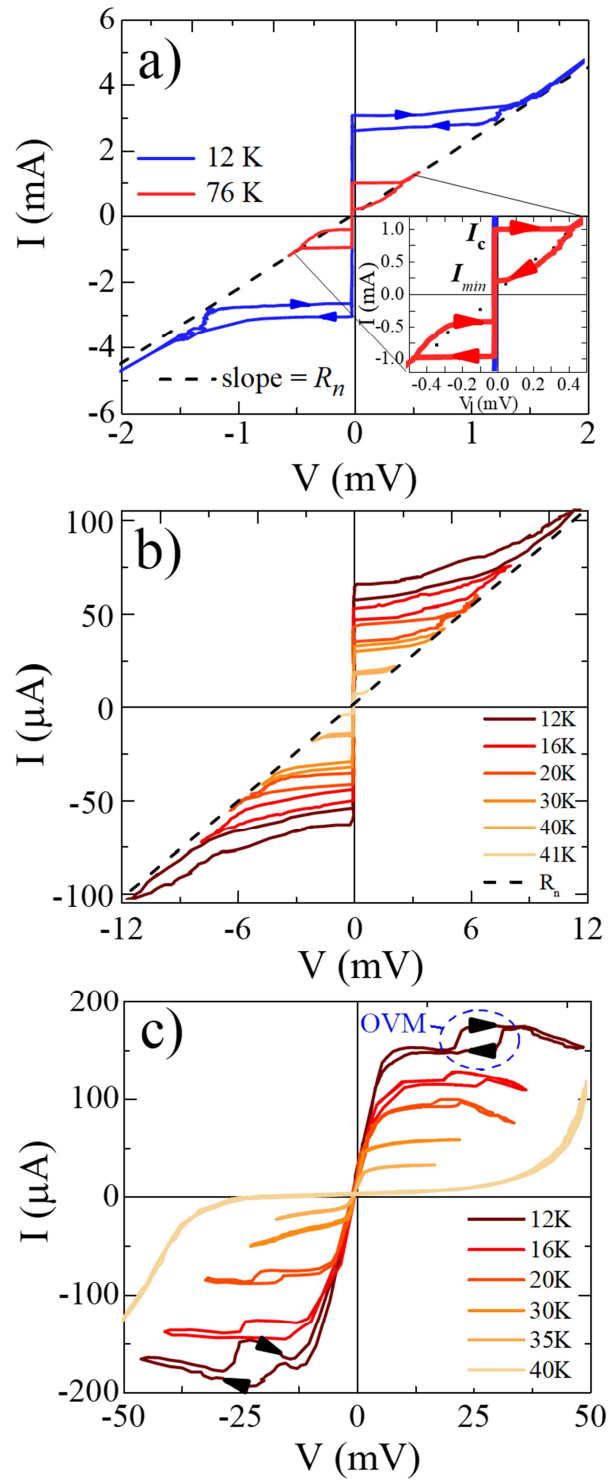


Figure 5.

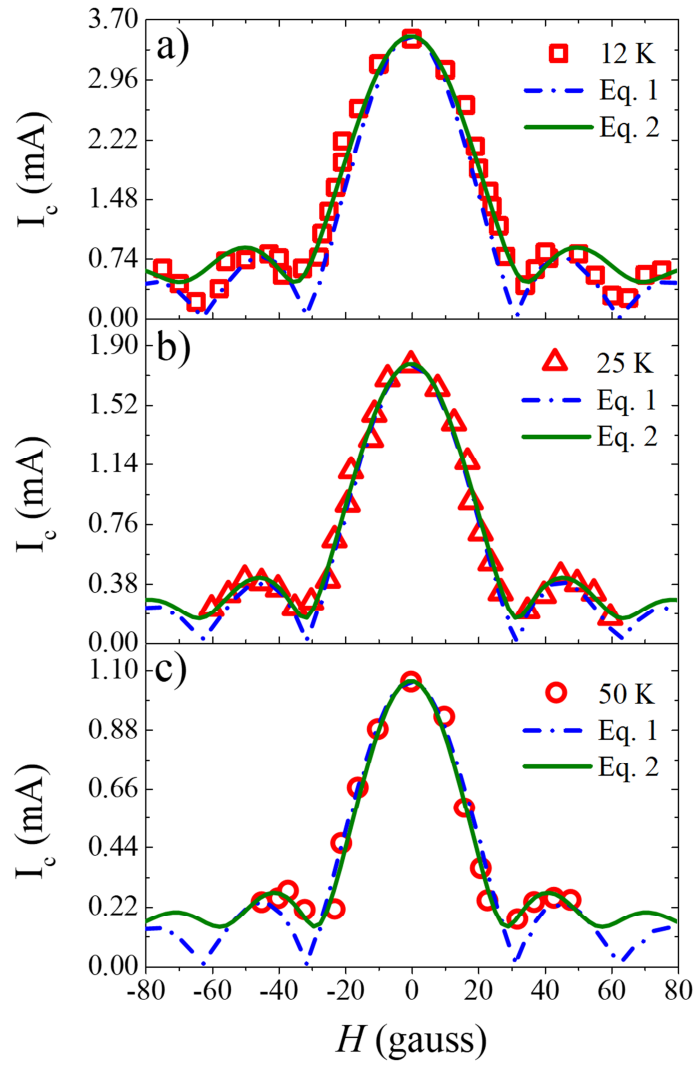
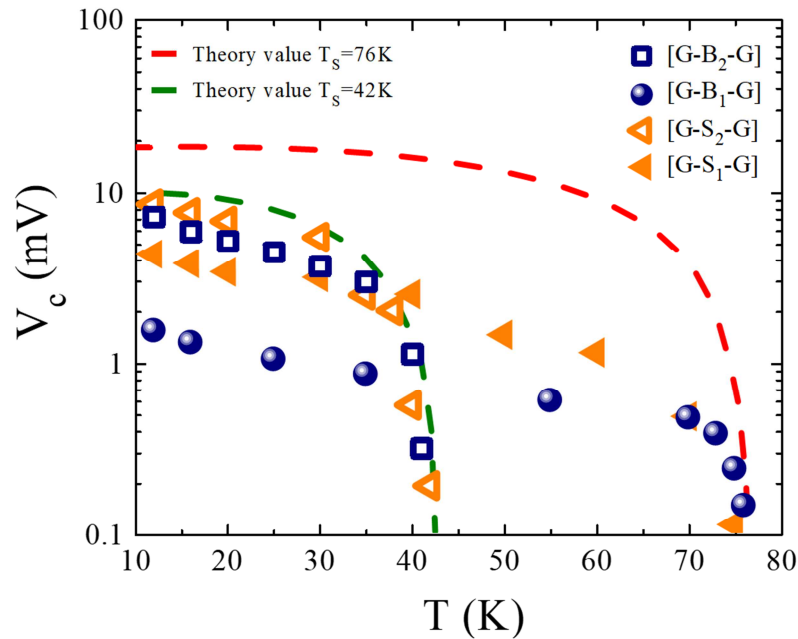


Figure 6.



- [1] Shane A. Cybart, E. Y. Cho, T. J. Wong, Björn H. Wehlin, Meng K. Ma, Chuong Huynh, R. C. Dynes. *Nature Nanotech* **10** (2015) 598-602. <https://doi.org/10.1038/nnano.2015.76>
- [2] Aleksander Divochiy, Francesco Marsili, David Bitauld, Alessandro Gaggero, Roberto Leoni, Francesco Mattioli, Alexander Korneev, Vitaliy Seleznev, Nataliya Kaurova, Olga Minaeva, Gregory Gol'tsman, Konstantinos G. Lagoudakis, Moushab Benkhaoul, Francis Lévy, Andrea Fiore. *Nature Photonics* **2** (2008) 302–306. <https://doi.org/10.1038/nphoton.2008.51>
- [3] S. J. Berkowitz, W. J. Skocpol, P. M. Mankiewich, R. H. Ono, N. Missert, P. A. Rosenthal, L. R. Vale. *J. Appl. Phys* **76** (1994) 1337-1339. <https://doi.org/10.1063/1.357798>
- [4] W. Booij, A. Pauza, E. Tarte, D. Moore, M. Blamire. *Phys. Rev. B* **55** (1997) 14600-14609. <https://doi.org/10.1103/PhysRevB.55.14600>
- [5] P. Chaudhari, J. Mannhart, D. Dimos, C. C. Tsuei, J. Chi, M. W. Oprysko, M. Scheuermann. *Phys. Rev. Lett* **60** (1988) 1653-1656. <https://doi.org/10.1103/PhysRevLett.60.1653>.
- [6] H. Hilgenkamp, J. Mannhart. *Rev. Mod. Phys* **74** (2002) 485-549. <https://doi.org/10.1103/RevModPhys.74.485>
- [7] S. Babcock, X. Cai, D. Kaiser, D. Larbalestier. *Nature* **347** (1990) 167-169. <https://doi.org/10.1038/347167a0>.
- [8] K. Hirata, K. Yamamoto, K. Iijima. *Appl. Phys. Lett.* **56** (1990) 683–685. <https://doi.org/10.1063/1.103311>
- [9] T. Kusumori, I. Iguchi. *Jpn J. Appl. Phys.* **31** (1992) L956–L959. <https://doi.org/10.1143/JJAP.31.L956>.

-
- [10] M. A. Bari, F. Baudenbacher, J. Santiso, E. J. Tarte, J. E. Evetts, M. G. Blamire. *Physica C* **256** (1996) 227–235. [https://doi.org/10.1016/0921-4534\(95\)00659-1](https://doi.org/10.1016/0921-4534(95)00659-1)
- [11] H. Navarro, M. Sirena, N. Haberkorn. *Nanotechnology* **31** (2020) 105701. <https://doi.org/10.1088/1361-6528/ab59f7>
- [12] M. J. A. Stoutimore, A. N. Rossolenko, V. V. Bolginov, V. A. Oboznov, A. Y. Rusanov, D. S. Baranov, N. Pugach, S. M. Frolov, V. V. Ryazanov, D. J. Van Harlingen. *Phys. Rev. Lett.* **121** (2018) 177702. <https://doi.org/10.1103/PhysRevLett.121.177702>
- [13] V. Rouco *et al.* *Nature. Comm.* **11** (2020) 658. <https://doi.org/10.1038/s41467-020-14379-w>
- [14] Jamie Wilt, Youpin Gong, Ming Gong, Feifan Su, Huikai Xu, Ridwan Sakidja, Alan Elliot, Rongtao Lu, Shiping Zhao, Siyuan Han, Judy Z. Wu. *Phys. Rev. Appl.* **7** (2017) 064022. <https://doi.org/10.1103/PhysRevApplied.7.064022>
- [15] H. Navarro, M. Sirena, J. Kim, N. Haberkorn. *Physica C* **510** (2015) 21-26. <https://doi.org/10.1016/j.physc.2014.12.010>.
- [16] Kun Li, Zheng Wen, Di Wu, Haifa Zhai, Aidong Li. *J. Phys. D: Appl. Phys.* **46** (2013) 035308. <https://doi.org/10.1088/0022-3727/46/3/035308>.
- [17] N. Haberkorn, F. Lovey, A. M. Condó, J. Guimpel. *J. Appl. Phys.* **97** (2005) 053511. <https://doi.org/10.1063/1.1858059>
- [18] Z. Wang, H. Terai, W. Qiu, K. Makise, Y. Uzawa, K. Kimoto, Y. Nakamura. *Appl. Phys. Lett.* **102** (2013) 142604. <https://doi.org/10.1063/1.4801972>
- [19] Ke Chen, C. G. Zhuang, Qi Li, Y. Zhu, P. M. Voyles, X. Weng, J. M. Redwing, R. K. Singh, A. N. Kleinsasser, X. X. Xi. *Appl. Phys. Lett.* **96** (2010) 042506. <https://doi.org/10.1063/1.3298366>
- [20] D. Massarotti, R. Caruso, A. Pal, G. Rotoli, L. Longobardi, G. P. Pepe M. G. Blamire, F. Tafuri. *Physica C* **533** (2017) 53-58. <https://doi.org/10.1016/j.physc.2016.07.018>
- [21] B. Börcsök, S. Komori, A. I. Buzdin, J. W. A. Robinson. *Scientific Reports* **9** (2019) 5616. <https://doi.org/10.1038/s41598-019-41764-3>
- [22] J. Müller, T. S. Böске, D. Bräuhaus, U. Schröder, U. Böttger, J. Sundqvist, P. Kücher, T. Mikolajick, L. Frey. *Appl. Phys. Lett.* **99** (2011) 112901. <https://doi.org/10.1063/1.3636417>
- [23] A. Crassous, R. Bernard, S. Fusil, K. Bouzehouane, D. Le Bourdais, S. Enouz-Vedrenne, J. Briatico, M. Bibes, A. Barthélémy, J. Villegas. *Phys. Rev. Lett.* **107** (2011) 247002. <https://doi.org/10.1103/PhysRevLett.107.247002>
- [24] Yuewei Yin, Qi Li. *J. Materiom.* **3** (2017) 245–254. <https://doi.org/10.1016/j.jmat.2017.09.001>
- [25] W. Guichard, M. April, O. Bourgeois, T. Kontos, J. Lesueur, P. Gandit. *Phys. Rev Lett.* **90** (2003) 167001. <https://doi.org/10.1103/PhysRevLett.90.167001>
- [26] C. H. Ahn, J. Triscone, J. Mannhart. *Nature* **424** (2003) 1015–1018. <https://doi.org/10.1038/nature01878>
- [27] H. Kohlstedt, N. A. Pertsev, J. Rodríguez Contreras, R. Waser. *Phys. Rev. B* **72** (2005) 125341. <https://doi.org/10.1103/PhysRevB.72.125341>

-
- [28] V. V. Lemanov, E. P. Smirnova, P. P. Syrnikov, and E. A. Tarakanov. *Phys. Rev. B* **54** (1996) 3151. <https://doi.org/10.1103/PhysRevB.54.3151>
- [29] H. Béa, S. Fusil, K. Bouzehouane, M. Bibes, M. Sirena, G. Herranz, E. Jacquet, J.-P. Contour, A. Barthélémy. *Jpn. J. Appl. Phys.* **45** (2006) L187. <https://doi.org/10.1143/JJAP.45.L187>
- [30] M. Sirena, L. Avilés, N. Haberkorn. *Appl. Phys. Lett.* **103** (2013) 052902. <https://doi.org/10.1063/1.4816416>
- [31] H. Navarro, Y. Yang, M. Sirena, J. Kim, N. Haberkorn. *J. Appl. Phys.* **118** (2015) 045308. <https://doi.org/10.1063/1.4927751>
- [32] H. Navarro, M. Sirena, J. González Sutter, H. E. Troiani, P. G. del Corro, P. Granell, F. Golmar, N. Haberkorn. *Mater. Res. Express* **5** (2018) 016408. <https://orcid.org/0000-0003-2899-1953>
- [33] Weiming Lü, Changjian Li, Limei Zheng, Juanxiu Xiao, Weinan Lin, Qiang Li, Xiao Renshaw Wang, Zhen Huang, Shengwei Zeng, Kun Han, Wenxiong Zhou, Kaiyang Zeng, Jingsheng Chen, Ariando, Wenwu Cao, Thirumalai Venkatesan. *Adv. Mater.* **29** (2017) 1606165. <https://doi.org/10.1002/adma.201606165>
- [34] G. Blatter, M. V. Feigelman, V. G. Geshkenbein, A. I. Larkin, V. M. Vinokur. *Rev. Mod. Phys.* **66** (1994) 1125-1388. <https://doi.org/10.1103/RevModPhys.66.1125>
- [35] Antonio Barone, Gianfranco Paterno. 1982, *Physical and Applications of the Josephson effect*, A Willey-Interscience Publication. John Wiley & Sons
- [36] Javier Junquera, Philippe Ghosez. *Nature* **422** (2003) 506–509. <https://doi.org/10.1038/nature01501>
- [37] I. K. Yanson. *Soviet Physics JETP* **31** (1970) 800
- [38] Elias Galan, Daniel Cunnane, X X Xi, Ke Chen. *Supercond. Sci. Technol.* **27** (2014) 065015. <https://doi.org/10.1088/0953-2048/27/6/065015>
- [39] A. Carrington, F. Manzano. *Physica C* **385** (2003) 205-214. [https://doi.org/10.1016/S0921-4534\(02\)02319-5](https://doi.org/10.1016/S0921-4534(02)02319-5)
- [40] A. M. Gabovich, A. I. Voitenko. *Low. Temp. Phys.* **40** (2014) 816. <https://doi.org/10.1063/1.4894415>
- [41] G. Burnell, D.-J Kang, H. N. Lee, S. H. Moon, B. Oh, M. G. Blamire. *Appl. Phys. Lett.* **79** (2001) 3464. <https://doi.org/10.1063/1.1419041>
- [42] N. Bergeal, J. Lesueur, M. Sirena, G. Faini, M. Aprili, J. P. Contour, B. Leridon. *J. Appl. Phys* **102** (2007) 083903. <https://doi.org/10.1063/1.2796105>
- [43] E. E. Mitchell, C. P. Foley. *Supercond. Sci. Technol.* **23** (2010) 065007. <https://doi.org/10.1088/0953-2048/23/6/065007>